Antihydrogen physics: gravitation and spectroscopy in AEgIS [1]

R. Ferragut, A.S. Belov, G. Bonomi, I. Boscolo, R.S. Brusa, V.M. Byakov, L. Cabaret, A. Calloni, C. Canali, C. Carraro, F. Castelli, S. Cialdi, D. Comparat, G. Consolati, L. Dassa, N. Djourelov, M. Doser, G. Drobychev, A. Dudarev, A. Dupasquier, G. Ferrari, A. Fischer, P. Folegati, A. Fontana, L. Formaro, M.G. Giammarchi, S.N. Gninenko, R. Heyne, S.D. Hogan, L.V. Jorgensen, A. Kellerbauer, D. Krasnicky, V. Lagomarsino, G. Manuzio, S. Mariazzi, V.A. Matveev, C. Morhard, G. Nebbia, P. Nedelec, M.K. Oberthaler, D. Perini, V. Petracek, F. Prelz, M. Prevedelli, I.Y. Al-Qaradawi, F. Quasso, C. Riccardi, O. Rohne, A. Rotondi, M. Sacerdoti, H. Sandaker, D. Sillou, S.V. Stepanov, H.H. Stroke, G. Testera, D. Trezzi, A.V. Turbabin, R. Vaccarone, F. Villa, U. Warring, S. Zavatarelli, A. Zenoni, and D.S. Zvezhinskij

Received 23 July 2010. Accepted 4 November 2010. Published on the NRC Research Press Web site at cjp.nrc.ca on .

R. Ferragut[2] and G. Consolati. Istituto Nazionale di Fisica Nucleare, via Celoria 16, 20133 Milano, Italy; Department of Physics, Politecnico di Milano, piazza L. da Vinci 32, 20133 Milano, Italy.
A.S. Belov, S.N. Gninenko, V.A. Matveev, and A.V. Turbabin. Institute for Nuclear Research of the Russian Academy of Sciences, Moscow 117312, Russia.
G. Bonomi, L. Dassa, A. Fontana, C. Riccardi, A. Rotondi, and A. Zenoni. Istituto Nazionale di Fisica Nucleare and Department of Physics, University of Pavia, via Bassi 6, 27100 Pavia, Italy.
I. Boscolo, F. Castelli, S. Cialdi, L. Formaro, D. Trezzi, and F. Villa. Istituto Nazionale di Fisica Nucleare, via Celoria 16, 20133 Milano, Italy; Department of Physics, University of Milan, via Celoria 16, 20133 Milano, Italy.
R.S. Brusa and S. Mariazzi. Department of Physics, University of Trento, via Sommarive 14, 38100 Povo, Italy.
V.M. Byakov. Institute for Theoretical and Experimental Physics, Moscow 117218, Russia.
L. Cabaret, D. Comparat, S.V. Stepanov, and D.S. Zvezhinskij. Laboratoire Aimé Cotton, CNRS, Université Paris-Sud, Bâtiment 505, 91405 Orsay, France.
A. Calloni, A. Dupasquier, P. Folegati, and F. Quasso. Department of Physics, Politecnico di Milano, piazza L. da Vinci 32, 20133 Milano, Italy.
C. Canali, A. Fischer, R. Heyne, A. Kellerbauer, C. Morhard, and U. Warring. Max Planck Institute for Nuclear Physics, Postfach 103980, 69029 Heidelberg, Germany.
C. Carraro, D. Krasnicky, V. Lagomarsino, G. Manuzio, G. Testera, R. Vaccarone, and S. Zavatarelli. Istituto Nazionale di Fisica Nucleare and Department of Physics, University of Genoa, via Dodecaneso 33, 16146 Genova, Italy.
N. Djourelov. Institute for Nuclear Research and Nuclear Energy, 72 Tzarigradsko Chaussee, 1784 Sofia, Bulgaria.
M. Doser, A. Dudarev, and D. Perini. Department of Physics, CERN, 1211 Geneva 23, Switzerland.
G. Drobychev, P. Nedelec, and D. Sillou. Lab. d'Annecy-le-Vieux de Phys. des Particules, 9 Chemin de Bellevue, B.p. 110, 74941 Annecy CEDEX, France.
G. Ferrari and M. Prevedelli. Istituto Nazionale di Fisica Nucleare, LENS-University of Florence, INO-CNR, via Sansone 1, 50019 Firenze, Italy.
M.G. Giammarchi and F. Prelz. Istituto Nazionale di Fisica Nucleare, via Celoria 16, 20133 Milano, Italy.
S.D. Hogan. Laboratorium für Physikalische Chemie, ETH Zürich, Zürich 8093, Switzerland.
L.V. Jorgensen and I.Y. Al-Qaradawi. Qatar University, Doha, Qatar P.O. Box 2713, Doha, Qatar.
G. Nebbia. Istituto Nazionale di Fisica Nucleare and Department of Physics, University of Padova, via Marzolo 8, 35131 Padova, Italy.
M.K. Oberthaler. Kirchhoff Institute of Physics, University of Heidelberg, Im Neuenheimer Feld 227, 69120 Heidelberg, Germany.
V. Petracek. Czech Technical University in Prague, Faculty of Nuclear Sciences and Physical Engineering.
O. Rohne. Department of Physics, University of Oslo, Boks 1072 Blindern, NO-0316 Oslo, Norway.
M. Sacerdoti. Department of Physics, University of Milan, via Celoria 16, 20133 Milano, Italy.
H. Sandaker. Department for Physics and Technology, University of Bermen, Allegaten 55, NO-5007 Bergen, Norway.
H.H. Stroke. Department of Physics, New York University, 4 Washington Place, New York, NY 10003, USA.

[1]This paper was presented at the International Conference on Precision Physics of Simple Atomic Systems, held at École de Physique, les Houches, France, 30 May – 4 June, 2010.
[2]Corresponding author (e-mail: Rafael.ferragut@polimi.it).

Abstract: AEgIS (Antimatter experiment: gravity, interferometry, spectroscopy) is an experiment approved by CERN with the goal of studying antihydrogen physics. In AEgIS, antihydrogen will be produced by charge exchange reactions of cold antiprotons with positronium atoms excited in a Rydberg state ($n > 20$). In the first phase of the experiment, controlled acceleration by an electric field gradient (Stark effect) and subsequent measurement of free fall in a Moiré deflectometer will allow a test of the weak equivalence principle. In a second phase, the antihydrogen will be slowed, confined, and laser-cooled to perform CPT studies and detailed spectroscopy. In the present work, after a general description of the experiment, the present status of advancement will be reviewed, with special attention to the production and excitation of positronium atoms.

PACS Nos: 03.75.Dg, 06.30.Gv, 25.43.+t, 34.80.Lx

Résumé : AEgIS (Expérience sur l'Antimatière: Gravité, Interférométrie, Spectrométrie) est une expérience approuvée par le CERN qui vise une étude globale de la physique de l'anti-hydrogène. Dans AEgIS, l'anti-hydrogène sera produit par des réactions d'échange de charges d'anti-protons froids avec des atomes de positronium excités dans un état de Rydberg ($n > 20$). Dans la première phase de l'expérience, l'accélération est contrôlée par un gradient de champ électrique (effet Stark); une mesure subséquente en chute libre dans un déflectomètre de Moiré nous fournira un test du principe d'équivalence faible. Dans une deuxième phase, l'anti-hydrogène sera ralenti, confiné et refroidi par laser pour des études de CPT et de spectroscopie de précision. Après une description générale de l'expérience, nous passons ici en revue l'état d'avancement des travaux en accordant une attention particulière à la production et l'excitation des atomes de positronium.

[Traduit par la Rédaction]

1. Introduction

A new generation of antimatter experiments has been opened after the first experiments of antihydrogen production in laboratory conditions at the CERN laboratory [1] and at Fermilab [2]. These experiments produced hot $\bar{H}$, i.e., relativistic, in small quantities not suited to precision $\bar{H}$ studies. Following that, a program is underway at CERN with a facility dedicated to low-energy $\bar{p}$ and $\bar{H}$ experiments. After the first production of cold $\bar{H}$ by the ATHENA [3, 4] and ATRAP [5, 6] collaborations, second-generation experiments, as ALPHA [7] and ASACUSA [8], are being performed to measure the fundamental properties of this antiatom. AEgIS is an experiment approved by CERN with the goal of studying $\bar{H}$ physics [9].

Some fundamental questions of modern physics relevant to the unification of gravity with the other fundamental interactions, models involving vector and scalar gravitons, matter–antimatter symmetry can be enlightened via experiments with antimatter [10]. A quantum theory of gravitation necessarily constitutes a departure from the Einstein view of gravity as a geometric phenomenon and could potentially constitute a violation of the weak equivalence principle. This principle is a foundation of General Relativity, and a large experimental effort is in place to test its consequences in all possible fields: this research activity includes tests of the equality of the inertial and gravitational mass, the universality of free fall, the search for non-Newtonian corrections to the gravitational law, the measurement of the gravitational red shift, and the search for time variation of the fundamental constants. Measurements studying the equality of the inertial and gravitational mass of different macroscopic bodies or cold atoms have only been performed on ordinary matter. There are no direct measurements of the validity of the principle of equivalence for antimatter. At present, the validity of the equivalence principle for antimatter is extrapolated from the matter results, or it is inferred using indirect arguments. Particularly interesting is that some quantum gravity models leave room for possible violations of the equivalence principle for antimatter [11]. Modern theories of gravity that attempt to unify gravity with the other forces of nature allow that, at least in principle, antimatter may fall differently from normal matter in the Earth's gravitational field. Specifically, as pointed out by Sherk [12], theories of supergravity are open to the possibility of a gravitational interaction that have different couplings for matter and antimatter.

The recent production of copious amounts of cold antihydrogen $\bar{H}$ at CERN's antiproton decelerator (AD) [3, 13] has paved the way for high-precision gravity experiments with neutral antimatter. In the first phase of the experiment, acceleration in a controlled way by an electric field gradient (Stark effect) and subsequent measurement of free fall in a Moiré deflectometer will allow a test of the weak equivalence principle. In a second phase, the antihydrogen will be slowed, confined, and laser-cooled to perform CPT studies and detailed spectroscopy.

Fig. 1 shows a schematic drawing of the basic experimental setup that should reach an accuracy of 1% in the measurement of the matter–antimatter gravitational acceleration. The experiment is designed to allow higher precision measurements through radial cooling of the beam [15]. The essential steps leading to the production of antihydrogen ($\bar{H}$) and the measurement of its gravitational interaction in AEgIS with the use of CERN cold antiproton ($\bar{p}$) are the following: (*i*) accumulation of positrons (e^+) in a Surko-type source and trap [16]; (*ii*) capture and accumulation of $\bar{p}$ from the AD in a cylindrical Penning–Malberg trap [17]; (*iii*) cooling of the $\bar{p}$ cloud to sub-K temperatures; (*iv*) production of cold positronium (Ps) by bombardment of a cryogenic nanoporous material with an intense e^+ pulse; (*v*) two-steps laser excitation of Ps to a Rydberg state (Ps*) with principal quantum number $n > 20$; (*vi*) pulsed formation of cold Rydberg antihydrogen $\bar{H}^*$ by means of the resonant charge exchange interaction between Rydberg Ps* and cold $\bar{p}$ with a residual electron: $Ps^* + \bar{p} \rightarrow \bar{H}^* + e^-$; (*vii*) pulsed

Fig. 1. Sketch of the experimental setup region where antiprotons and positrons are manipulated to form and to accelerate antihydrogen. This region is at low temperature (~100 mK) in an axial magnetic field of 1 T [14].

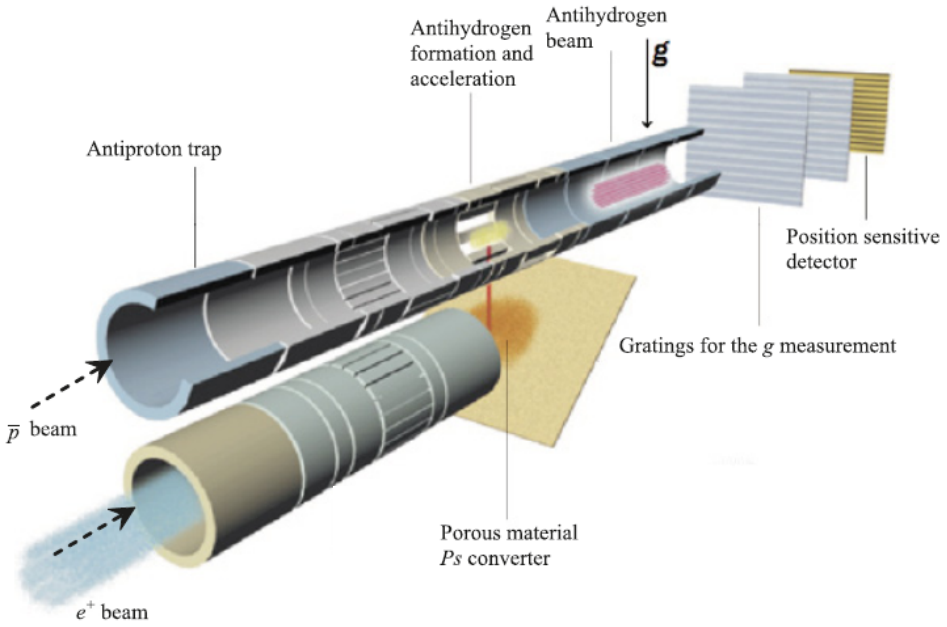

formation of an $\bar{H}^*$ beam by Stark acceleration with inhomogeneous electric fields; (*viii*) determination of g in a two-grating Moiré deflectometer coupled with a position-sensitive detector.

In the present work, the status of advancement will be reviewed, with special attention to the production and excitation of positronium atoms.

2. Method

2.1. Positronium formation

There are several models of Ps formation, which were reviewed in [18]. Ground-state Ps is formed as 75% ortho-Ps (spin 1) and 25% para-Ps (spin 0). Para-Ps annihilates in two γ rays of 511 keV each, and ortho-Ps in vacuum is required to annihilate into three γ rays at least, with a maximum energy of 511 keV each and with a total energy of 1022 keV ($2m_0c^2$). We are interested only in Ps emitted by the converter as ortho-Ps with a characteristic lifetime in vacuum of 142 ns, since the lifetime of para-Ps is too short (125 ps) to allow the necessary laser excitation before annihilation. The ortho-Ps lifetime can be shortened by collisional pick-off annihilation and ortho-para conversion (both processes lead to annihilation in two γ rays) in ranges typically from a fraction of a nanosecond to tens of nanoseconds.

A magnetic field mixes the two substates of Ps with $m=0$, the levels with $m=\pm1$ remaining unaltered [19]. This leads to annihilation into two γ rays of the $m=0$ ortho-Ps state; the effect is normally called ortho-Ps magnetic quenching, since the lifetime of $m=0$ ortho-Ps is decreased ("quenched") by the magnetic field. In our experiment, the Ps converter (Fig. 1) will be located in a 1 T magnetic field [20].

A strategy to obtain Ps in vacuum is to use porous materials with pores open to the surface. Porous materials are necessary not only to form a high yield of Ps atoms but also to cool Ps through collisions with the inner walls of the pores. Ps atoms are emitted from the pore walls with high kinetic energy (1–3 eV) [21]. The collisions between Ps and the internal surface of the pores involve weak coupling to phonons or other surface modes. Ps formation and cooling has been extensively discussed in [22]. Low Ps kinetic energies are desirable for AEgIS. The velocity distribution of the Ps atoms coming out of the target should be of the order of 10^4 ms^{-1} to allow Ps laser excitation to a Rydberg state (Ps*) and for efficient $\bar{H}$ formation, which requires that the relative velocity of antiprotons and Ps* must be similar to or lower than the classical orbital velocity of the positron in the Rydberg Ps atom [15, 23, 24]. Efficient formation of cooled Ps atoms is a requisite for the production of antihydrogen. The thermalization of Ps atoms is possible by means of hundreds of thousands of collisions with the walls of the pores. A careful choice of the materials used to convert bare positrons in Ps atoms is required to provide the appropriate morphology for efficient cooling. Not only is the morphology of the pores at nanometric scale an important aspect, but so is the chemical composition of the pore walls. Fig. 2 shows schematic views of two nanometric porous solids, which represent two alternative strategies for AEgIS: samples with wide and interconnected random pores [25] and ordered structures with SiO_2 at the surface of the pores [26]. Ps time of flight (Ps-TOF) measurements in silicon nanochannels (5–8 nm in diameter) with a well-controlled oxidized surface (SiO_2) show escaping and cooling of Ps by collisions with the walls of nanochannels at 150 K [26]. Ps quantum confinement limits the minimum achievable positronium energy in vacuum. For a typical pore dimension of 10 nm, a velocity distribution with a minimum of about 10^4 ms^{-1} is expected. Measurements of the ortho-Ps emission energy in

Fig. 2. Schematic views of systems formed by nanometric solids interspersed with empty regions: (*a*) a random structure in a disordered SiO_2 skeleton (e.g., silica Aerogel or compressed powder); (*b*) ordered nanochannels with SiO_2 at the surface.

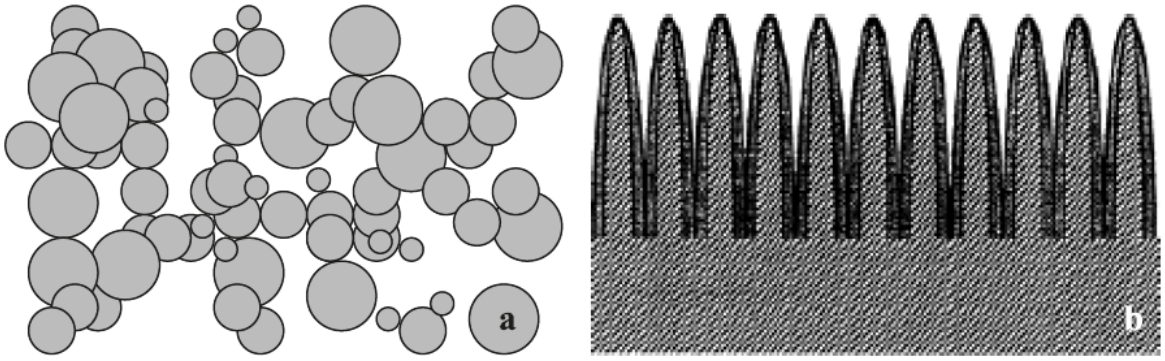

vacuum from mesoporous silica films using Ps-TOF were reported in [27], where the results show evidence of quantum mechanical confinement in the mesopores that define the minimal energy of the emitted Ps. A similar work is underway with Aerogel samples. In contrast to the proposed schemes in [26, 27] in aligned pores, in this case an isotropic spatial distribution of velocities of Ps escaping into vacuum is expected due to the absence of a preferential confinement direction in a random structure.

Figure 3 shows the 3γ fraction $F_{3\gamma}$ as a function of the positron implantation energy in an Aerogel sample with a density of 150 mg cm^{-3} [25]. The Ps yield in Aerogel is very high at all implantation energies. Mills et al. [28] observed ortho-Ps thermalization also at low temperature in SiO_2 compressed powder (180 mg cm^{-3}). The results of [28] indicate: 2% at 4.2 K, 8% at 77 K, and 12% at 300 K of thermal ortho-Ps with positron implantation energies of 19, 10, and 7 keV, respectively. These high implantation energies require rather thick samples (several microns, for typical Aerogel densities), which is a condition easily met with homogenous Aerogel. However a compromise must be reached between efficient cooling, which requires deep positron implantation, and high ortho-Ps yield outside the target, which is favoured by implantation depths not large in comparison with the ortho-Ps diffusion length. In the case of Aerogel, the ortho-Ps diffusion length is expected to be some microns [25, 29].

The AEgIS experiment will be performed at cryogenic temperatures (100 mK). The low temperature of the sample contributes to Ps thermalization [25, 26]. Figure 4 shows the Ps yield as a function of the temperature in a Xerogel sample (a variant of Aerogel) of 85 mg cm^{-3} for positrons implanted in the sample at 3 keV [29]. These results indicate that in silica-based materials the high Ps production does not depend on temperature. A similar result was found in silica films [27]. A negative aspect of the cryogenic environment is the formation of ice at the surface of the pores, as well as in ultra-high vacuum conditions [30]. An ice cap could avoid the Ps escape in the free space outside the target. Ice formation at the surface of the Ps converter represents an important subject of further studies.

2.2. Positronium excitation

Antihydrogen production by charge exchange reaction between Ps atoms and antiprotons is the main process consid-

Fig. 3. Positronium 3γ fraction $F_{3\gamma}$ measured at room temperature as a function of the positron implantation energy in Aerogel with a density of 150 mg cm^{-3} [25]. The dashed line is only a visual guide. Error bar is shown for one point.

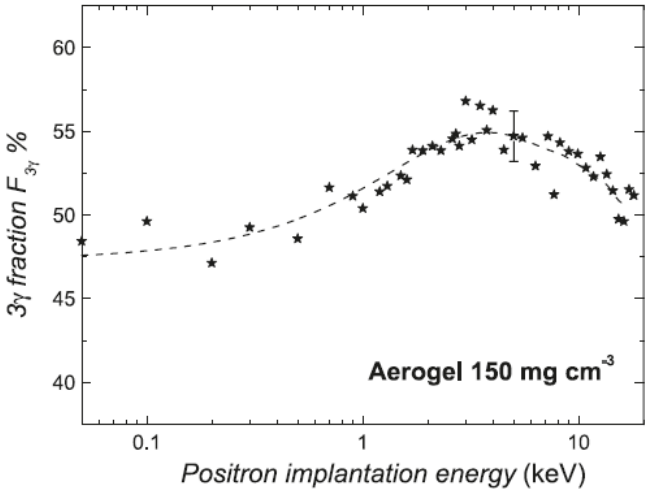

Fig. 4. Positronium 3γ fraction $F_{3\gamma}$ as a function of the temperature for positron implanted inside the sample at 3 keV in Xerogel 85 mg cm^{-3} [29].

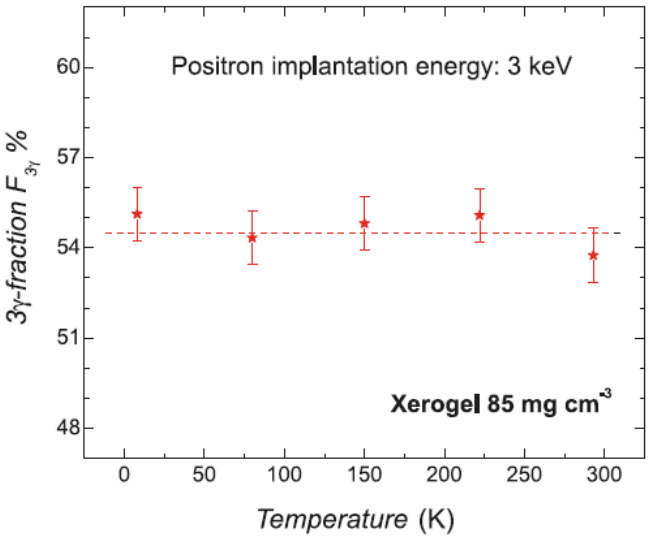

ered for antimatter production in AEgIS. Since the cross-section for this reaction depends roughly on n^4, an efficient laser excitation is being developed to pump Ps atoms up to high-n levels (Rydberg levels), as has been suggested by Charlton [31]. A Ps cloud will be produced by positrons hitting a porous silica target in a relatively strong uniform magnetic field (1 T, see Sect. 2.1). The experimental strategy involves exciting Ps into Rydberg states in two steps, one from $n=1$ to $n=3$, which involves radiation at 205 nm, and a second one from $n=3$ to 20...30, involving radiation in the range 1600–1700 nm. The two laser sources share similar requirements in terms of spectral properties, as discussed in [32, 33], and adopt related technical solutions.

The main features of this two-step excitation are the significant Doppler effect for the first transition and the modifications due to Zeeman and motional Stark effects on the high-n sublevel structure [33]. The pump laser of the whole system will be a 650 mJ Q-switched Nd:YAG laser delivering a 4 ns pulse. The radiation is produced through second-order polarization in optical crystals (see Fig. 5). The 205 nm radiation for the first transition is obtained by summing in a nonlinear BBO crystal the 266 nm fourth-harmonic of the 1064 nm Nd:YAG pulse and the 894 nm radiation generated in an optical parametric generator (OPG) by down-conversion of the second harmonic of the same laser. The other wavelength (around 1670 nm) is generated in a single step by an OPG starting from the same pump laser and then amplified by an optical parametric amplifier (OPA) system.

The system has been completely designed and is partly completed. The energy required to saturate this second transition of 174 μJ [33] has been exceeded, having currently reached 3 mJ after an OPA using a temporary Nd:YAG laser of only 80 mJ energy per pulse. The stability in space and in energy of the produced pulse is now studied with the goal of optimizing the system. The laser system at 205 nm, responsible for the excitation $n=1\rightarrow 3$, has the following requirements: (*i*) spectral bandwidth larger than 150 GHz RMS, mainly accounting for the Doppler broadening, with a continuum, non-discrete spectrum (see [33]); (*ii*) a pulse duration shorter than 10 ns; (*iii*) an integrated energy in the range of 100 μJ or larger.

The requirements on the spectral properties and the pulse duration are easily fulfilled by using an OPG pumped by a Q-switched pump laser, but those on the wavelength and the energy per pulse are not so trivial to fulfil. In fact, producing 205 nm photons by direct parametric down-conversion is not realistic because of the lack of suitable pump lasers at wavelengths shorter than 205 nm. Alternative approaches based on harmonic generation, such as frequency doubling or tripling, of parametrically down-converted photons at longer wavelength are not viable mainly because of the limited efficiency attainable in the harmonic process. Given these constraints, a different approach will be considered, based both on parametric down-conversion and frequency summing processes. Here, the first requirement is satisfied by generating radiation at 894 nm with an OPG pumped by a nanosecond frequency doubled Nd:YAG laser at 532 nm. Subsequently, the 894 nm light is frequency summed to the second harmonic of the same pump laser at a wavelength of 266 nm, hence generating 205 nm radiation. Compared with the case of direct harmonic generation of the OPG-generated radiation, with our approach the conversion process towards 205 nm is considerably more effective because of the large amount of energy available at 266 nm with nanosecond lasers, which boosts the nonlinear conversion towards the deep UV. From the spectral point of view, the frequency summing process consists in adding the continuous spectrum from the OPG to the comb-like spectrum of the 266 nm radiation (obtained as the fourth harmonic of a Q-switched Nd:YAG lasers), hence resulting in the required continuous spectrum peaked at 205 nm. A sketch of the laser setup under development is depicted in Fig. 5. A visible beam splitter sends about 3 mJ of the 532 nm pulse to the OPG1, generating 894 nm radiation, while the remainder is sent to a second frequency doubling stage, which converts about 15 mJ to 266 nm. The OPG1 is based on a 30 mm long periodically-poled KTP crystal that ensures conversion efficiency towards 894 nm of about 10% when pumping with pulses of 3 mJ, hence resulting in pulses of about 300 μJ in the infrared. Finally, the frequency summing stage is composed of a dichroic mirror superposing the radiations at 894 and 266 nm, which is followed by a RR cut to satisfy the type-I phase matching condition for the process, 894 nm + 266 nm → 205 nm, and 3 mm long to insure a nonlinear conversion bandwidth larger than 150 GHz for frequency tuning of the infrared radiation. It is possible to obtain about 200 μJ at 205 nm on a spectrum fulfilling the specifications discussed above.

2.3. Antihydrogen beam formation

As presented in Subsects. 2.1 and 2.2, Ps atoms emitted from the porous insulator material are excited to Rydberg states. They then traverse a Penning trap region in which $\sim 10^5$ $\bar{p}$ have been accumulated, stored, and cooled. The low-temperature requirement on the antiprotons comes from the requirement that the antihydrogen atoms that form will have a transverse velocity that is low compared with the velocity of several 100 ms^{-1} that they will achieve after acceleration. To reach such a low temperature, the Penning trap is coupled to a 50 mK dilution refrigerator, and the antiprotons are coupled to the low-temperature environment by embedding them in an electron plasma. The latter will cool down through synchrotron radiation, as well as through a tuned circuit; furthermore, evaporative cooling of the precooled antiprotons is envisaged [34]. The charge exchange cross-section is very large ($\sim 10^7$ $Å^2$ for $n=35$) and reaches a maximum when the e^+ and $\bar{p}$ relative velocities are matched [15]. Taking into account the corresponding kinetic energy, as well as a smaller contribution due to converted internal energy, $\bar{H}$ will be created at velocities of 25–80 ms^{-1}.

The neutral atoms are not sensitive (to first order) to constant electric fields, but they do experience a force when their electric dipole moment is exposed to an electric-field gradient. Since the dipole moment scales approximately with the square of the principal quantum number, Rydberg atoms are especially amenable to being manipulated in this way [14, 35]. Such so-called Stark acceleration (and deceleration) has been successfully demonstrated, among others, by one of the AEgIS groups with (ordinary) hydrogen after excitation to the $n=22$, 23, 24 states [36, 37]. In these experi-

Fig. 5. Sketch of the setup for the laser excitation of Rydberg Ps. The $n = 1 \rightarrow 3$ exciting laser at 205 nm. The $n = 3 \rightarrow 20 \ldots 30$ exciting laser at about 1670 nm.

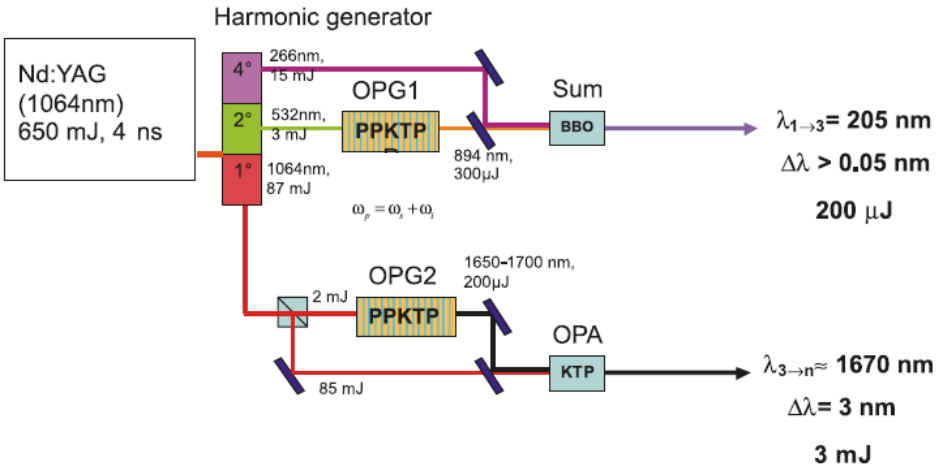

ments, accelerations of 2×10^8 ms^{-2} were achieved using two pairs of electrodes at right angles to each other. A hydrogen beam travelling at 700 ms^{-1} was stopped within 5 μs over a distance of only 1.8 mm. We intend to use a similar field configuration, generated by axially split electrodes within the cylindrical geometry of a Penning trap, to accelerate the formed $\bar{H}$ atoms to about 400 ms^{-1} in the direction of the deflectometer apparatus.

2.4. Gravity measurement

Consider a beam of antihydrogen that falls freely in the Earth's gravitational field. Given AEgIS realistic numbers, flight path length of 1 m, horizontal velocity of about 500 ms^{-1}, the vertical displacement of an antihydrogen atom due to gravity, assuming $g = 10$ ms^{-2}, would be about 20 μm. However, when created, the antihydrogen has a thermal velocity in all directions of a few tens of ms^{-1} (corresponding to the 100 mK at which the $\bar{H}$ production will take place). In other words, the beam has a large radial divergence. During the flight path, an antihydrogen atom can thus displace vertically up to 10 cm, and it is not possible for each anti-atom to know its radial velocity. On top of that, the vertical position of the antihydrogens when leaving the Stark acceleration region is known with a precision of 1 mm. It is therefore clear that it is impossible to measure the gravitational acceleration g by simply measuring the vertical displacement. The solution to such problem resides in the so called Moiré deflectometer that has been successfully used to measure the gravitational acceleration g with a beam of argon atoms [38]. This system is purely classical, since it is based on geometric propagation of an (anti)atomic beam through a set of identical gratings. In its original form it consisted of three material gratings, equally spaced and aligned parallel to each other, while in the AEgIS configuration (see Fig. 6) the third grating is replaced by a position-sensitive $\bar{H}$ annihilation detector. The first two gratings select propagation directions of an originally diverging atomic beam. Beyond such gratings, the atoms are distributed in a shadow image forming sets of fringes at various distances from the second grating, multiples of the distance between

Fig. 6. Configuration of the Moiré deflectometer consisting of two gratings coupled to a position-sensitive detector [40].

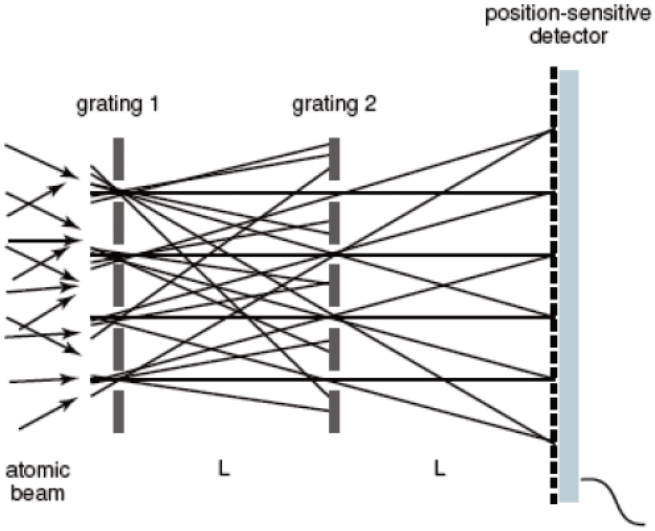

the first two gratings. This device is nondispersive, in the sense that atoms with a broad energy distribution and without collimation can be used. If the atom beam is in accelerated motion, as in a gravitational field, a fringe shift of the shadow image equal to $\delta = -gT^2$ will be induced, where T is the time of flight between two adjacent gratings. This time can be calculated since both the starting time (Stark acceleration) and the stopping time (annihilation) are known with a precision much smaller than the typical time of flight of few ms. Since our beam will not be monochromatic, this time of flight is not constant but will be characterized by a given distribution. Nevertheless the antihydrogens can be grouped in bins of different velocities, and the corresponding δ can be measured. A parabolic fit to δ as a function of the averaged time of flight $\sqrt{T^2}$ in each bin with a function of the type $\delta_0 + g\,T^2$, can deliver the measure of the acceleration constant g; δ_0, whose value is provided by the fit itself, ac-

counts for possible geometrical misalignment between the gratings.

More details about the position-sensitive detector are presented in [39, 40].

3. Summary and outlook

As discussed in Subsects. 2.1 and 2.2, the formation and excitation of Ps to a Rydberg state represents a very interesting challenge. Our proposed technique of $\bar{H}$ formation is conceptually similar to a charge exchange technique based on Rydberg Cs [24], which has been successfully demonstrated by ATRAP [41], but offers greater control of the final state distribution of $\bar{H}$ and allows pulsed production of $\bar{H}$.

Construction has started on the AEgIS experiment, whose design is based upon the broad experience gained with the ATHENA and ATRAP experiments at the AD, a series of ongoing related experiments, tests and developments, as well as extensive simulations of critical processes (charge exchange production of $\bar{H}$, Stark acceleration and propagation through the Moiré deflectometer, resolution of the position-sensitive detector located at the end of the deflectometer). The proposed gravity measurement merges in a single experimental apparatus technologies already demonstrated or based on reasonable additional development.

For the initial phase of the experiment, obtaining samples of anti-atoms at 100 mK is an essential requirement. Gravity measurements with even higher precision, as well as competitive CPT tests through spectroscopy, are desirable, but will necessitate the development of novel techniques to attain even colder $\bar{H}$ ensembles. The experiment has been designed with flexibility of the apparatus in mind, to allow a number of techniques, which may lead to such physics topics, to be implemented. One natural extension of the modular design is to incorporate, in a future stage, a magnetic decelerator and trap for $\bar{H}$, which will be spatially separated from the region where the anti-atoms are produced, similar to the devices currently being used to trap and study H atoms [42, 43]. The experience gained in the first phase of AEgIS with the formation of a $\bar{H}$ beam will be used to optimize the design of such a trapping system.

References

1. G. Baur, G. Boero, A. Brauksiepe, A. Buzzo, W. Eyrich, R. Geyer, D. Grzonka, J. Hauffe, K. Kilian, M. LoVetere, et al. Phys. Lett. **368B**, 251 (1996).
2. G. Blanford, D.C. Christian, K. Gollwitzer, M. Mandelkern, C.T. Munger, J. Schultz, and G. Zioulas. Phys. Rev. Lett. **80**, 3037 (1998). doi:10.1103/PhysRevLett.80.3037.
3. M. Amoretti, C. Amsler, G. Bonomi, A. Bouchta, P. Bowe, C. Carraro, C.L. Cesar, M. Charlton, M.J.T. Collier, M. Doser, V. Filippini, K.S. Fine, A. Fontana, M.C. Fujiwara, R. Funakoshi, P. Genova, J.S. Hangst, R.S. Hayano, M.H. Holzscheiter, L.V. Jørgensen, V. Lagomarsino, R. Landua, D. Lindelöf, E.L. Rizzini, M. Macrì, N. Madsen, G. Manuzio, M. Marchesotti, P. Montagna, H. Pruys, C. Regenfus, P. Riedler, J. Rochet, A. Rotondi, G. Rouleau, G. Testera, A. Variola, T.L. Watson, and D.P. van der Werf;? ATHENA Collaboration. Nature, **419**, 456 (2002). doi:10.1038/nature01096.
4. ATHENA. Available from http://athena.web.cern.ch/athena/.
5. G. Gabrielse, et al. ATRAP Collaboration. Phys. Lett. **507B**, 1 (2001).
6. ATRAP. Available from http://hussle.harvard.edu/~atrap/.
7. ALPHA. Available from http://alpha.web.cern.ch/alpha/.
8. ASACUSA. Available from http://asacusa.web.cern.ch/asacusa/.
9. AEgIS. Available from http://aegis.web.cern.ch/aegis/.
10. R.J. Hughes. Nucl. Phys. A. **558**, 605 (1993). doi:10.1016/0375-9474(93)90423-U.
11. M. Nieto and T. Goldman. Phys. Rep. **205**, 221 (1992). doi:10.1016/0370-1573(91)90138-C.
12. J. Sherk. Phys. Lett. **88B**, 265 (1979).
13. G. Gabrielse, N.S. Bowden, P. Oxley, A. Speck, C.H. Storry, J.N. Tan, M. Wessels, D. Grzonka, W. Oelert, G. Schepers, T. Sefzick, J. Walz, H. Pittner, T.W. Hänsch, and E.A. Hessels; ATRAP Collaboration. Phys. Rev. Lett. **89**, 213401 (2002). doi:10.1103/PhysRevLett.89.213401.
14. G. Testera, et al. AEgIS Collaboration. Proceedings of Cold Antimatter Plasmas and Application to Fundamental Physics Conference (Okinawa), Vol. 1037, AIP Conference Proceedings, 2008. p. 5.
15. AEgIS proposal available from http://cdsweb.cern.ch/record/1037532/files/spsc-2007-017.pdf.
16. T.J. Murphy and C.M. Surko. Phys. Rev. A, **46**, 5696 (1992). doi:10.1103/PhysRevA.46.5696.
17. J.H. Malmberg and C.F. Driscoll. Phys. Rev. Lett. **44**, 654 (1980). doi:10.1103/PhysRevLett.44.654.
18. O.E. Mogensen. Positron annihilation in chemistry. Springer-Verlag, Berlin. 1995.
19. O. Halpern. Phys. Rev. **94**, 904 (1954). doi:10.1103/PhysRev.94.904.
20. A. Bisi, A. Fiorentini, E. Gatti, and L. Zappa. Phys. Rev. **128**, 2195 (1962). doi:10.1103/PhysRev.128.2195.
21. Y. Nagashima, Y. Morinaka, T. Kurihara, Y. Nagai, T. Hyodo, T. Shidara, and K. Nakahara. Phys. Rev. B, **58**, 12676 (1998). doi:10.1103/PhysRevB.58.12676.
22. R.S. Brusa and A. Dupasquier. *In* Physics with many positrons. *Edited by* R.S. Brusa, A. Dupasquier, and A.P. Mills, Jr. IOS Press, Amsterdam. 2010. pp. 245–296.
23. T.F. Gallagher. Rep. Prog. Phys. **51**, 143 (1988). doi:10.1088/0034-4885/51/2/001.
24. E.A. Hessels, D.M. Homan, and M.J. Cavagnero. Phys. Rev. A, **57**, 1668 (1998). doi:10.1103/PhysRevA.57.1668.
25. R. Ferragut, A. Calloni, A. Dupasquier, G. Consolati, F. Quasso, M.G. Giammarchi, D. Trezzi, W. Egger, L. Ravelli, M.P. Petkov, S.M. Jones, B. Wang, O.M. Yaghi, B. Jasinska, N. Chiodini, and A. Paleari. J. Phys: Conf. Ser. **225**, 012007 (2010). doi:10.1088/1742-6596/225/1/012007.
26. S. Mariazzi, P. Bettotti, and R.S. Brusa. Phys. Rev. Lett. **104**, 243401 (2010). doi:10.1103/PhysRevLett.104.243401.
27. P. Crivelli, L. Liszkay, P. Perez, and C. Corbel. Phys. Rev. A, **81**, 052703 (2010). doi:10.1103/PhysRevA.81.052703.
28. A.P. Mills, Jr., E.D. Shaw, R.J. Chichester, and D.M. Zuckerman. Phys. Rev. B, **40**, 2045 (1989). doi:10.1103/PhysRevB.40.2045.
29. R. Ferragut, et al., J. Phys.: Conf. Ser. (2011). Manuscript in Press.
30. O. Sneh, M.A. Cameron, and S.M. George. Surf. Sci. **364**, 61 (1996). doi:10.1016/0039-6028(96)00592-4.
31. M. Charlton. Phys. Lett. **143A**, 143 (1990).
32. M.G. Giammarchi, et al. AEgIS Collaboration. Hyperfine Interact. **193**, 321 (2009). doi:10.1007/s10751-009-0018-5.
33. F. Castelli, I. Boscolo, S. Cialdi, M.G. Giammarchi, and D.

Comparat. Phys. Rev. A, **78**, 052512 (2008). doi:10.1103/PhysRevA.78.052512.
34. G.B. Andersen, et al. ALPHA Collaboration. Phys. Rev. Lett. **105**, 013003 (2010). doi:10.1103/PhysRevLett.105.013003.
35. M. Doser and A. collaboration. J. Phys: Conf. Ser. **199**, 012009 (2010). doi:10.1088/1742-6596/199/1/012009.
36. E. Vliegen and F. Merkt. J. Phys. B, **39**, L241 (2006). doi:10.1088/0953-4075/39/11/L03.
37. E. Vliegen, S.D. Hogan, H. Schmutz, and F. Merkt. Phys. Rev. A, **76**, 023405 (2007). doi:10.1103/PhysRevA.76.023405.
38. M.K. Oberthaler, S. Bernet, E.M. Rasel, J. Schmiedmayer, and A. Zeilinger. Phys. Rev. A, **54**, 3165 (1996). doi:10.1103/PhysRevA.54.3165.
39. G. Bonomi, et al. AEgIS Collaboration. Hyperfine Interact. **193**, 297 (2009). doi:10.1007/s10751-009-0015-8.
40. A. Kellerbauer, M. Amoretti, A. Belov, G. Bonomi, I. Boscolo, R. Brusa, M. Buchner, V. Byakov, L. Cabaret, and C. Canali. AEgIS Collaboration. Nucl. Instrum. Methods Phys. Res. Sect. B, **266**, 351 (2008). doi:10.1016/j.nimb.2007.12.010.
41. C.H. Storry, A. Speck, D. Sage, N. Guise, G. Gabrielse, D. Grzonka, W. Oelert, G. Schepers, T. Sefzick, H. Pittner, M. Herrmann, J. Walz, T. Hänsch, D. Comeau, and E. Hessels. ATRAP Collaboration. Phys. Rev. Lett. **93**, 263401 (2004). doi:10.1103/PhysRevLett.93.263401.
42. S. Hogan and F. Merkt. Phys. Rev. Lett. **100**, 043001 (2008). doi:10.1103/PhysRevLett.100.043001.
43. S. Hogan, A. Wiederkehr, H. Schmutz, and F. Merkt. Phys. Rev. Lett. **101**, 143001 (2008). doi:10.1103/PhysRevLett.101.143001.